Observation of double isovector giant dipole resonances from pion double charge exchange

S. Mordechai
Ben-Gurion University of the Negev, Beer-Sheva 84105, Israel
and University of Texas at Austin, Austin, Texas 78712

H. T. Fortune, J. M. O'Donnell, G. Liu, M. Burlein, and A. H. Wuosmaa
University of Pennsylvania, Philadelphia, Pennsylvania 19104

S. Greene and C. L. Morris
Los Alamos National Laboratory, Los Alamos, New Mexico 87545

N. Auerbach
Tel Aviv University, Tel Aviv, Israel

S. H. Yoo and C. Fred Moore
University of Texas at Austin, Austin, Texas 78712
(Received 28 August 1989)

We report the observation of double isovector giant dipole resonances in (π^+, π^-) and, for the first time, also in (π^-, π^+) double-charge-exchange reactions at $T_\pi = 292$ MeV. The resonances have been observed on nine targets covering a wide range of mass at Q values around ≈ -50 MeV in (π^+, π^-), but at significantly lower energy ($Q = -33.8$ MeV) in the inverse reaction on ^{56}Fe. The centroid energies in both reactions are very close to the energies at which the $\Delta T_z = \pm 2$ double giant dipole ($J^\pi = 0^+, 2,^+, \Delta T = 2$) states are expected to appear. Angular distributions have been measured for the (π^+, π^-) resonances on ^{40}Ca, ^{56}Fe, and ^{93}Nb and each is observed to have a quadrupole shape. Based on their energies, angular distributions, cross sections, and the comparison between the (π^+, π^-) and (π^-, π^+) data on ^{56}Fe, we identify the resonances as double giant dipole states (i.e., states arising from a charge-exchange dipole operator acting twice on the ground-state wave function). The data from the present and recent observations indicate that the newly discovered resonance is a general collective feature of all nuclei.

I. INTRODUCTION

In a recent paper[1] we reported the first observation of a double isovector giant-dipole state in nuclei via the pion double-charge-exchange reaction (DCX) on ^{nat}S. The identification of the resonance was based on the energy centroid, the characteristic angular distribution, and the cross section with which it was populated. The double giant dipole state can be written[2] in terms of a charge-exchange dipole operator, $D_\pm$, acting twice on the ground-state wave function:

$$|D_{\pm 1}; D_{\pm 1}\rangle = \sum_{i=1}^{A} r_i\, y_1(\theta_i)\, t_{\pm 1}(i)|D_{\pm 1}\rangle/N\,, \qquad (1)$$

where

$$|D_{\pm 1}\rangle = \sum_{i=1}^{A} r_i\, y_1(\theta_i)\, t_{\pm 1}(i)|0\rangle \qquad (2)$$

and $t_{\pm 1}$ are the usual isospin-raising and isospin-lowering operators, changing a proton into a neutron or vice versa, respectively, and N is a proper normalization factor. In principle, two isovector excitations can couple to $\Delta T = 0$, 1, or 2. However, in DCX reactions $\Delta T_z = \pm 2$ and therefore no isoscalar or isovector components are allowed, and only $\Delta T = 2$ transitions are accessible. Similarly, a coupling of two $\ell = 1$ multipoles gives a total angular momentum transfer $\Delta L = 0$, 1, or 2. However, for a two-identical-phonon wave function $\Delta T + \Delta L$ must be even and therefore only $\Delta L = 0$, 2 are allowed. This will also be the total J transfer for the double-dipole state in DCX, since $\Delta S = 0$ transitions dominate the spectra at forward angles. Thus, for example, for self-conjugate target nuclei the quantum numbers of the double dipole given in Eq. (1) are $J^\pi = 0^+, 2^+; T = 2$. The difficulty in observing double giant resonances arises from the fact that these states are expected to be high in the continuum region and superimposed on a large nonresonant background. Pion DCX offers a cleaner way to study double giant resonances than that offered by inelastic or

single-charge-exchange reactions, since the latter excite the isoscalar and isovector states—which are forbidden in DCX. One example of this unique feature of pion DCX as an excellent tool to study states arising from double multipole operators acting on the nuclear ground-state wave function is the well-known double isobaric analog state (DIAS) which is given by:

$$|A_2\rangle \equiv |A_1; A_1\rangle = T_{-1}^2|0\rangle/[(N-Z)(N-Z-1)]^{1/2} , \quad (3)$$

where A_1 is the isobaric analog state:

$$|A_1\rangle = T_{-1}|0\rangle/(N-Z)^{1/2} , \quad (4)$$

and $T_{-1} = \sum_{i=1}^{A} t_{-1}(i)$. Another example is the $\Delta T_z = -1$ component of the dipole state built on the isobaric analog state. This newly observed resonance[3,4] is given by

$$|D_{-1}; A_1\rangle = \sum_{i=1}^{A} r_i\, y_1(\theta_i)\, t_{-1}(i)|A_1\rangle/N. \quad (5)$$

Equation (5) describes the $\Delta T_z = -2$ component of a dipole built on the isobaric analog state labeled as GDR⊗IAS in Refs. 3 and 4.

The results from pion single charge exchange (SCX) show that the isobaric analog states (IAS) and the isovector giant dipole resonances (GDR) are the two most prominent features in the spectra.[5–7] They have both been observed in (π^+, π^0) [and the GDR also in (π^-, π^0)] with a typical maximum cross section of 0.5–1.0 mb/sr. The IAS is absent in all (π^-, π^0) as well as in (π^+, π^0) on $T=0$ targets. In both of these latter cases the GDR is the only prominent feature of the spectra. Pion double charge exchange involving the excitations of the closed-shell cores proceeds predominantly by a two-step sequential $(\pi^+, \pi^0)(\pi^0, \pi^-)$ mechanism, and therefore it was suggested that it should be a unique probe for exciting isotensor double giant resonances in nuclei.[2] The lowest in energy of these is the DIAS Eq. (3). The GDR built on the IAS or vice versa Eq. (5) is the second double resonance, and the GDR built on a GDR Eq. (1) is the third double resonance expected in pion DCX. The three double resonances have different quantum numbers and can be distinguished experimentally by measuring the characteristic angular distributions, the excitation energies and the cross sections of the resonances. In this work we report on new observations of the double isovector giant dipole resonances in (π^+, π^-) and, for the first time, also in the inverse (π^-, π^+) reaction. The results from the present and previous work[1] indicate that these resonances are a general feature of all nuclei. We will also discuss the energies, widths, and cross sections of these exotic states and compare their features in the $\Delta T_z = -2$ and +2 DCX modes.

II. EXPERIMENT

The measurements were performed using the energetic pion channel and spectrometer (EPICS) at the Clinton P. Anderson Meson Physics Facility (LAMPF) with the standard pion double-charge-exchange setup.[8] The isotopic purity and areal density of the targets used in the present and previous experiments are listed in Table I. Measurements were taken at $T_\pi = 292$ MeV and a scattering angle of 5°. Angular distributions were measured on ^{40}Ca, ^{56}Fe, and ^{93}Nb at scattering angles 5°–40°. Electrons were eliminated using a freon-gas velocity-threshold Cherenkov detector in the focal plane. A scintillator placed behind a series of graphite blocks was used to detect and veto muon events[9]. The system was fine tuned by placing aluminum absorbers of variable thickness in front of the first scintillator to ensure that no pions reached the veto scintillator. The remaining background was pions resulting from DCX to the continuum on the target. The choice of the highest beam energy available at EPICS ($T_\pi = 292$ MeV) for these measurements had three advantages: (a) a lower background level underneath the giant resonance peaks since the excitation-energy region of interest is further away from the inclusive DCX peak, (b) a large outgoing energy range (≈ 50 MeV) is covered by the acceptance of the spectrometer in a single setting, and (c) cross sections are expected to increase as k^2 or faster.

TABLE I. Target compositions and areal densities.

Target	Isotopic purity (%)	Areal density (g/cm^2)
^{12}C	98.9	2.212
^{13}C	90.0	0.329
^{32}S[a]	95.0	2.00
^{40}Ca	96.9	2.38
^{56}Fe	91.8	1.199
^{59}Co	100	1.079
^{93}Nb	100	1.714
^{138}Ba	>99	0.327
^{197}Au	100	1.000

[a] Reference 1.

The acceptance of the spectrometer was measured by pion scattering from ^{12}C at a given angle by varying the spectrometer field to cover an outgoing pion momentum range of about ±10% of the central momentum of the spectrometer. Absolute normalizations were obtained by measuring π-p scattering from a polyethylene (CH_2) target of areal density 25.7 mg/cm^2 and comparing the yields with cross sections calculated by π-nucleon phase shifts of Ref. 10.

III. RESULTS AND ANALYSIS

A. Discussion of the data

Figure 1 displays the ^{40}Ca(π^+, π^-) Q-value spectra at two angles, (a) 5° and (b) 40°. In addition to the ground state ($Q = -24.7$ MeV), the spectrum at 5° contains a wide peak labeled GR, located in the continuum region at about 26.4 MeV above the ground state. The resonance

is significantly weaker at the 40° spectrum. The giant resonance (GR) peak was fitted with a Lorentzian shape of variable width. The fit uses $\Gamma(\text{g.s.}) = 1.3$ MeV (arising from the resolution) and $\Gamma(\text{GR}) = 9.0$ MeV. The spectra have been corrected for the spectrometer acceptance as a function of momentum. The background (dashed line), which arises from the DCX cross section to discrete low-lying states and to the continuum, was fitted using a third-order polynomial function of the energy and will be discussed later. Comparable fits and cross sections are obtained if, instead, fourth- or higher-order polynomial shapes are used for the background. In order to reduce uncertainties from the choice of background, the same background form (third-order polynomial) was used at all angles. The variation of the fitted background with scattering angle and mass will be discussed in Sec. III B. The solid lines are the resulting fits to the spectra. Figure 2 presents the ^{93}Nb Q-value histograms at 5° and 20°. In addition to the DIAS ($T = \frac{11}{2}$) at $E_x = 19.3$ MeV ($Q = -21.9$ MeV) which is clear at 5°, the spectrum contains two wide peaks labeled GR1 and GR2 at about 33.2 and 47.3 MeV above the g.s. ($Q = -35.8$ and -49.9 MeV). The fit shown uses $\Gamma_{\text{DIAS}} = 0.8$ MeV, $\Gamma(\text{GR1}) = 5.8$ MeV, and $\Gamma(\text{GR2}) = 8.8$ MeV. At 20° GR1 vanishes but GR2 is almost as strong as in the 5° spectrum. The background (dashed line) is again a third-order polynomial shape. A quick comparison between the ^{40}Ca and ^{93}Nb DCX spectra shows some interesting features. The peak labeled GR2 in the ^{93}Nb spectra appears at about the same Q value as the GR on ^{40}Ca, whereas the lower peak labeled GR1 on ^{93}Nb is missing on ^{40}Ca. An additional obvious difference is, of course, that ^{40}Ca ($T = 0$) has no DIAS. Figure 3 shows the ^{56}Fe(π^+, π^-) DCX spectra at 12° and 25°. Again, in addition to the DIAS transition (which is very weak at the above angles, but is clear at the 5° spectrum shown later), one can identify two wide resonances at higher energies labeled GR1 and GR2. Clearly, the two resonances have a different nature since they have a significantly different angular dependence.

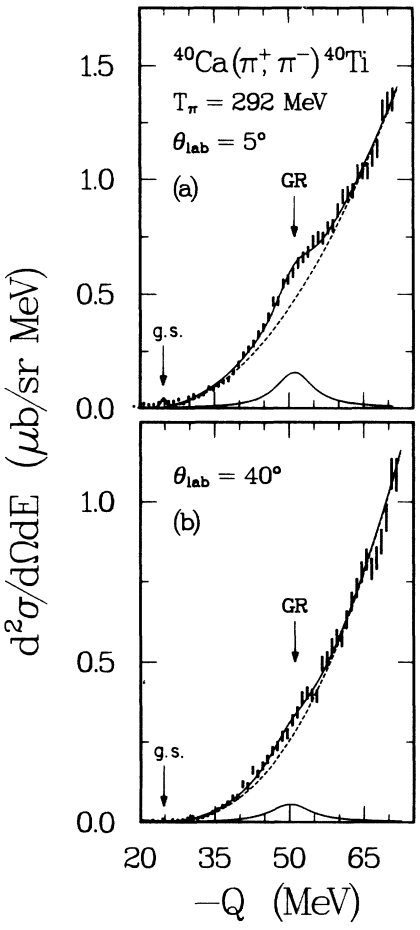

FIG. 1. (a) Double-differential cross-section spectrum for the (π^+, π^-) reaction on a ^{40}Ca target at $T_\pi = 292$ MeV and $\theta_{lab} = 5°$. The arrows indicate the fitted location of the ground state (g.s.) and the giant resonance (GR). Short vertical lines represent statistical uncertainties of the data. The dashed line is the fitted background with a polynomial shape and the solid line is the fit to the spectrum with the use of NEWFIT. (b) Same as (a) except for $\theta_{lab} = 40°$.

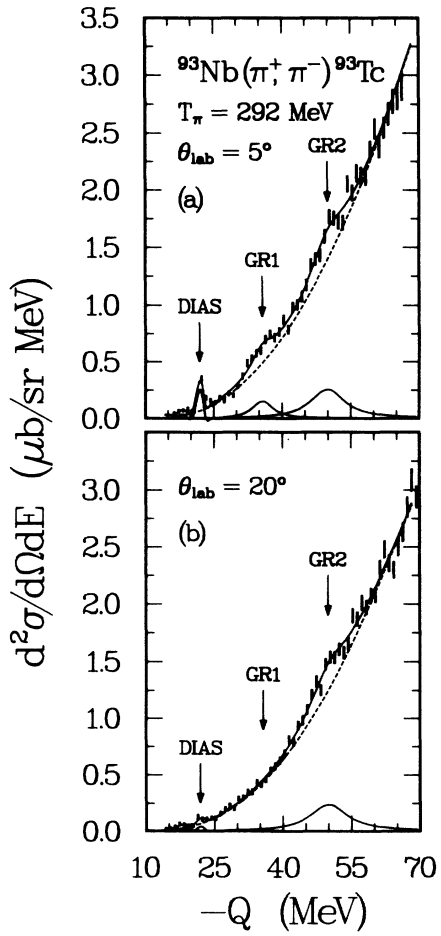

FIG. 2. (a) Same as Fig. 1 except for ^{93}Nb target at $\theta_{lab} = 5°$ and (b) $\theta_{lab} = 20°$. The arrows indicate the fitted locations of the DIAS, GR1, and GR2.

Figure 4(a) presents the angular distribution extracted for the GR peak on ^{40}Ca. Figs. 4(b) and (c) show the angular distribution for both GR1 and GR2 on ^{93}Nb and ^{56}Fe, respectively. The two resonances, GR1 and GR2, have different angular distributions. GR1 peaks around 10° and has a dipole shape, whereas the higher resonance (GR2) has a quadrupole distribution that is similar in shape and magnitude to the single GR peak observed on ^{40}Ca. In a previous communication we identify GR1 on ^{56}Fe, ^{93}Nb, and several other $T \geq 1$ targets as the giant dipole built on the isobaric analog state, GDR⊗IAS, and discuss their properties in detail.[11] The identification is based on the characteristic dipole angular distribution, the excitation energy, and the measured cross section. This resonance is absent on ^{40}Ca (and other self-conjugate targets in this study) because no IAS, and hence no GDR⊗IAS, is possible on a $T=0$ nucleus. In the following discussion we will concentrate mainly on the properties of the higher-energy resonance which appears around $Q=-50$ MeV in all the above spectra.

B. Background analysis

Table II lists the reduced χ^2 and the parameters, $R_i(\theta)$, of the third-order polynomial expansion for the background obtained from fitting the individual spectra on ^{40}Ca with two peaks—the ground state and a GR peak with a width of $\Gamma=9.0$ MeV. The fits for the 5° and 40° spectra shown in Fig. 1 are obtained with a constant energy for the peaks and constrained widths as listed

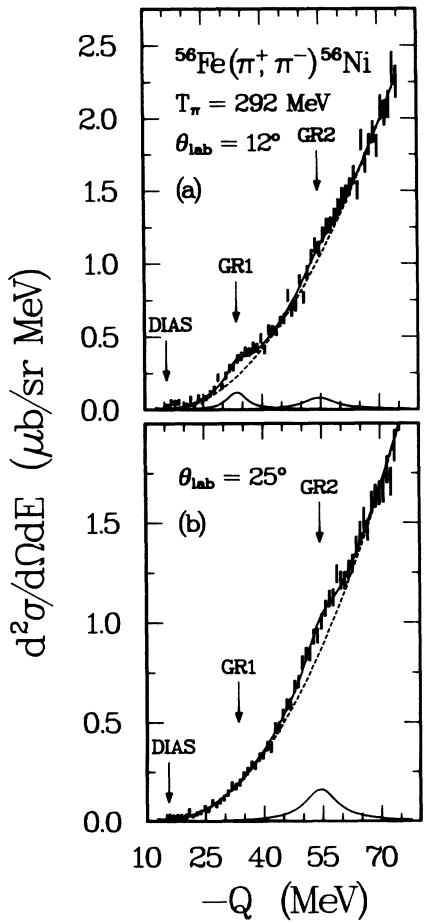

FIG. 3. (a) Same as Fig. 2 except for ^{56}Fe(π^+, π^-)^{56}Ni spectra at $\theta_{lab}=12°$ and (b) $\theta_{lab}=25°$.

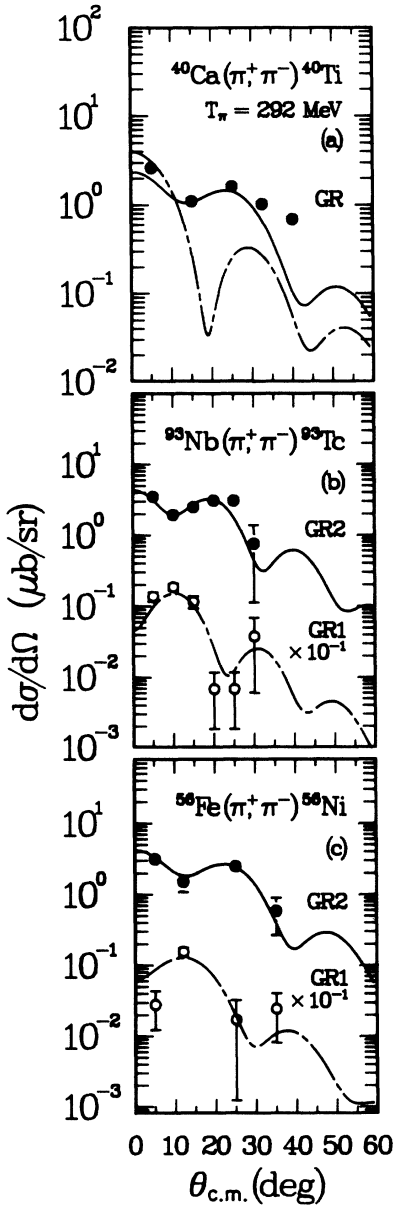

FIG. 4. (a) Angular distribution for the peak labeled GR in the double-charge-exchange spectra on ^{40}Ca shown in Fig. 1. The cross sections have been extracted with use of a Lorentzian line shape for the giant resonance with constant width of 9.0 MeV and constant $Q=-51.1$ MeV. The solid curve is from a sequential-model calculation for the double-dipole ($J^\pi=2^+$) state, but renormalized as mentioned in the text. The chain-dashed curve for the double-dipole ($J^\pi=0^+$) state is shown without any normalization factor. (b) and (c) The same as (a) except for ^{93}Nb(π^+, π^-) and ^{56}Fe(π^+, π^-) reactions. The solid and chain-dashed lines are the theoretical calculations for the double dipole and the dipole built on the isobaric analog state, respectively.

TABLE II. Parameters of the polynomial background [see Eq. (6)] obtained from fitting the ^{40}Ca(π^+, π^-)^{40}Ti spectra with and without a giant-resonance peak assumed in the fit.

No. of peaks [a]	θ (deg)	q^2 [b] (fm^{-2})	χ^2 [c]	R_1	R_2 $\times 10^1$	R_3 $\times 10^3$	R_4 $\times 10^5$
1	5	0.10	1.19	0.16±0.04	−0.14±0.04	0.24±0.11	0.28±0.09
1	15	0.33	0.98	0.25±0.05	−0.19±0.05	0.31±0.13	0.30±0.11
1	25	0.77	1.61	0.17±0.03	−0.14±0.03	0.19±0.09	0.32±0.08
1	32.5	1.25	1.38	0.07±0.03	−0.03±0.03	−0.11±0.08	0.52±0.07
1	40	1.82	1.17	0.10±0.03	−0.06±0.03	−0.016±0.08	0.38±0.07
0	5	0.10	4.31	0.45±0.03	−0.42±0.03	1.09±0.07	−0.46±0.06

[a] In addition to the ground state.
[b] Momentum transfer at the region of the giant-resonance peak ($Q = -51.1$ MeV).
[c] Reduced χ^2 for the entire histogram.

earlier. Also shown in Table II, for comparison, are the χ^2 and the background parameters obtained from fitting the 5° spectra with no GR peak. Fitting the spectrum with the unrealistic case of no GR peak gives a significantly larger χ^2. However, except for an overall upwards shift the background shape is affected very little by the preceding assumption.

It is interesting to compare the background in shape and magnitude at different angles using the fitted values of $R_i(\theta)$ listed in Table II. Using the above values one can compute the background for each angle using the polynomial expansion:

$$\text{Background}(E,\theta) = R_1(\theta) + R_2(\theta)E + R_3(\theta)E^2 + R_4(\theta)E^3 , \quad (6)$$

where E is minus the Q value in MeV.

Figure 5 shows a plot of the background computed using Eq. (6) for the ^{40}Ca(π^+, π^-)^{40}Ti reaction. Except for the 5° spectrum the background decreases smoothly with scattering angle. This feature may arise from the small shift of the whole inclusive DCX spectra toward lower energies with increasing scattering angle.[12,13] An exception to this behavior is found in the 5° spectrum, where the background level is lower than for 15°, in contrast to the preceding systematic dependence. The overall lowering (at large missing mass) of the 5° differential cross sections relative to the 15° spectra was also observed in the DCX reaction on ^{93}Nb and may arise from Pauli blocking in changing two inner shell neutrons into protons in the (π^+, π^-)reaction at very small momentum transfer where such transitions are partially blocked.

One can choose some selective energy ($-Q$ value) bins around the GR's region in the background spectra of Fig. 5 and plot the background cross section as a function of θ for each of the energy bins. Figure 6 shows such a plot using 5-MeV binning size. The figure shows the absence of isotropy of the nonresonant background in the DCX spectra. The overall feature is the monotonic decrease of the background with scattering angle, except that the 5° cross sections seem to be strongly suppressed—perhaps due to Pauli blocking effects—especially at the higher excitation energies. If we extrapolate the nearly linear curves, we can estimate what the cross section at $\theta_{lab} = 5°$ would have been with no such suppression. Using the 47–52 and 52–57 MeV energy bins (which are located at the GR region) we estimate the Pauli blocking at 5° for this energy region to be larger than 30%. If the cross sections for the GR's are subject to the same amount of suppression as the underlying background, then the calculated cross sections at 5° plotted in Fig. 4 should decrease by 30% at least. For a given scattering angle (i.e., 5°) one can also study the variation of the background with mass. Such analysis indicates that the background shape has only a weak dependence upon A.

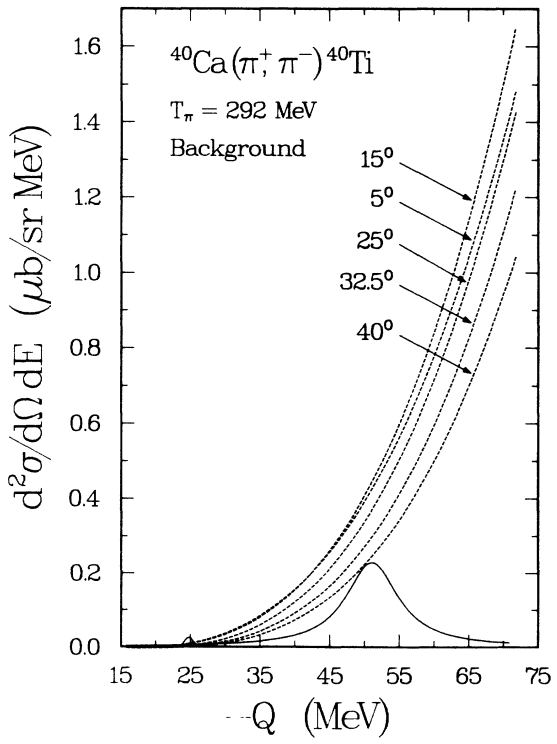

FIG. 5. Comparison between the fitted background for the ^{40}Ca(π^+, π^-)^{40}Ti spectra measured at 292 MeV and scattering angles of 5, 15, 25, 32.5, and 40°.

C. Sequential-model calculations

A simple sequential model has been used to predict the cross section and angular distribution for the double-dipole state. We used the pion coupled-channel impulse approximation code (CCIA) NEWCHOP.[14] The calculations for the double dipole include the ground state (g.s.), the giant dipole resonance (GDR), and the double dipole (GDR^2). A schematic diagram for a $T=0$ case is shown in Fig. 1 of Ref. 1. The collective model has been used to obtain the radial shape of the transition density for the dipole. The strength of each SCX has been adjusted to reproduce the measured or extrapolated (π^+, π^0) cross section for the GDR at 165 MeV.[15] The transition strength thus obtained was used at 292 MeV for both SCX processes. This method was tested against SCX data[16] at lower energies. Further details on the calculations for the double dipole and for the GDR built on the IAS can be found in Ref. 1 and Ref. 4, respectively.

The results of these calculations for the double dipole (solid line) and the giant dipole built on the isobaric analog state (chain-dashed line) shown in Figs. 4(b) and (c) give strong support to the identification of the lower and upper GR peaks on ^{56}Fe and ^{93}Nb as the giant dipole

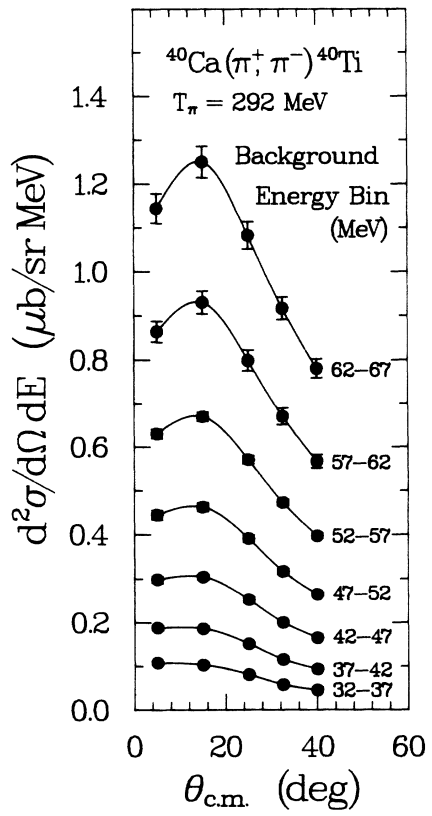

FIG. 6. Angular distribution of selective energy ($-Q$ value) bins in the background spectra in the ^{40}Ca(π^+, π^-)^{40}Ti reaction at T_π = 292 MeV shown in Fig. 5. The numbers to the right are the energy bins. The lines are smooth curves to guide the eye.

built on the isobaric analog (GDR⊗IAS) and the double-dipole (GDR^2) states, respectively. Similarly, we identify the single resonance on ^{40}Ca as the $T=2$, $J^\pi=2^+$ double-dipole state. If the energy difference between the double-dipole $J^\pi=0^+$ and 2^+ states is small, then we actually observe the sum of the two states. As mentioned in Sec. III B, the 5° cross sections are suppressed (by 30% at least) due to Pauli blocking. Our macroscopic impulse-approximation calculations use collective-transition densities for the dipole and do not include this blocking effect. Including this correction to the theory will shift the calculated 5° cross section downward and indicates that we may actually observe both the 0^+ and 2^+ spin members of the double giant dipole. The calculated cross section for the double dipole with J = 2 is found to peak near 0° and 22°, as would be expected for coupling of two dipoles, each peaking at this energy around 11°. The calculated solid curves for the double-dipole states shown in Fig. 4 have been multiplied by factors of 2.8 (^{40}Ca), 4.0 (^{93}Nb), and 3.5 (^{56}Fe) to normalize to the data. The chain-dashed curves for the $J^\pi=0^+$ double-dipole state Fig. 4(a) and the GDR⊗IAS [Figs. 4(b) and (c)] are shown without any renormalization factor.

D. Properties of the double giant dipole resonance

Table III summarizes the deduced energies, widths, and cross sections for the giant resonances from the present and previous studies. The data on ^{32}S is taken from Ref. 1 but refitted with a single peak under the same conditions, to examine the global features of these resonances. Also listed are the calculated cross sections for the double-dipole states from sequential-model calculations and energies and widths available from the SCX data for the GDR on nearby nuclei from Ref. 15. The energy centroid of GR1 on ^{56}Fe and ^{93}Nb is almost exactly at the energy expected for the giant dipole built on the IAS. This issue is addressed in detail in Ref. 11, where we show that the GDR energies derived from the GDR⊗IAS resonances are consistent with the corresponding $E1$ energies from photonuclear reactions. This resonance (as well as the IAS) is absent in all (π^-, π^+) data. In (π^+, π^0) SCX data[15] shown in Table III, the GDR appears at about 25 MeV. Its energy and cross section are very weakly dependent on A. If we assume that the second dipole has the same energy as the first dipole then

$$Q_{\mathrm{DCX}}(\mathrm{GDR}^2) = 2Q_{\mathrm{SCX}}(\mathrm{GDR}) \simeq -50\ \mathrm{MeV}.$$

This is surprisingly close to the energy at which the higher resonances are observed in the (π^+, π^-) reactions, although the approximation neglects the effect of isospin splitting.

A unique feature of pion DCX reactions is the simplicity with which one can study the $\Delta T_z=+2$ DCX mode, just by inverting the polarities of all magnets in the pion channel and the spectrometer. We utilized this feature in the present experiment in order to further examine the nature of these resonances. Figure 7 shows the mea-

TABLE III. Results from pion double-charge-exchange (π^+, π^-) reactions and (π^-, π^+) reactions on ^{56}Fe at an incident pion energy $T_\pi = 292$ MeV and a laboratory angle $\theta_{lab} = 5°$ compared with sequential-model calculations and pion single-charge-exchange data.

Reaction	Double charge exchange — Experiment[a]					σ(GDR^2)[b]		Single charge exchange[c]		
	Q(g.s./DIAS)[d] (MeV)	Q(GDR⊗IAS) (MeV)	Q(GDR^2) (MeV)	Γ(GDR^2) (MeV)	σ(GDR^2) (μb/sr)	0^+ (μb/sr)	2^+	Reaction	Q(GDR)[e] (MeV)	Γ(GDR) (MeV)
^{12}C(π^+, π^-)	−31.1±0.1	—	−48.4±2.0	10.0±3.0	0.86±0.18	5.43	1.09			
^{13}C(π^+, π^-)	−18.9±0.1	−27.4±0.5	−46.5±2.0	12.0±3.0	3.20±0.53	4.74	0.98			
^{32}S(π^+, π^-)	−22.8±0.1	—	−49.6±2.0	9.0±2.0	0.98±0.31	3.47	0.79			
^{40}Ca(π^+, π^-)	−24.7±0.1	—	−51.1±0.5	9.0±1.4	2.64±0.22	3.38	0.76	^{40}Ca(π^+, π^0)	−24.7±2.1	6.4±1.9
^{56}Fe(π^+, π^-)	−15.6±0.1	−34.7±0.6	−54.4±0.6	10.0±1.5	3.12±0.31	4.15	0.88	^{60}Ni(π^+, π^0)	−25.3±1.5	6.4±1.7
^{56}Fe(π^-, π^+)	−6.4±0.2	—	−33.8±0.8	8.0±2.0	1.05±0.22	0.78	0.20	^{60}Ni(π^-, π^0)	−13.5±1.6	4.2±2.0
^{59}Co(π^+, π^-)	−15.9±0.1	−32.3±1.1	−48.6±0.8	8.2±2.0	4.05±0.75	3.36	0.71			
^{93}Nb(π^+, π^-)	−21.9±0.1	−35.8±0.5	−49.9±0.8	8.8±2.6	3.48±0.47	4.58	0.89	^{90}Zr(π^+, π^0)	−25.7±1.2	6.0±1.7
^{138}Ba(π^+, π^-)	−27.38±0.07	−38.4±0.4	−49.8±0.8	8.5±2.6	4.15±0.52	4.62	0.82	^{120}Sn(π^+, π^0)	−23.9±0.9	3.4±2.1
^{197}Au(π^+, π^-)	−34.7±0.1	−46.0±0.8	−52.1±0.8	10.0±2.6	5.74±2.01	7.25	1.22	^{208}Pb(π^+, π^0)	(−26.5)	(6)

[a] Cross sections, energies, and widths for the double giant dipole obtained by fitting the GR with a single Lorentzian peak with the listed widths. Data from Ref. 1 have been refitted under the same conditions.

[b] Calculated cross sections for the 0^+ and 2^+ double-dipole states with use of the code NEWCHOP (Ref. 14) at 5° and $T_\pi = 292$ MeV.

[c] Data are taken from Ref. 15.

[d] Ground state Q value for ^{12}C(π^+, π^-), ^{13}C(π^+, π^-), ^{32}S(π^+, π^-), ^{40}Ca(π^+, π^-), and ^{56}Fe(π^-, π^+). DIAS Q value for ^{56}Fe(π^+, π^-), ^{59}Co(π^+, π^-), ^{93}Nb(π^+, π^-), ^{138}Ba, and ^{197}Au(π^+, π^-).

[e] Mass difference between the ground state and the charge-exchange GDR.

sured spectra and fits from (π^+, π^-), and (π^-, π^+) on ^{56}Fe at $\theta_{lab} = 5°$ under the same conditions. In (π^+, π^-) the lower resonance (GR1) (shown also in Fig. 3), which we identify from previous data[3] based on its energy and angular distributions as the giant dipole built on the isobaric analog state, is observed at $Q = -34.7$ MeV and the higher resonance (GR2), which we identify as the giant dipole built on the giant dipole, is observed at $Q = -54.4$ MeV. In the inverse reaction the GDR⊗IAS is absent and there is only one peak apparent at $Q = -33.8$ MeV. Figure 4(c) shows the angular distribution for GR1 and GR2 on ^{56}Fe from the (π^+, π^-) reaction. It is clear that GR2 has a quadrupole and GR1 has a dipole angular distribution.

The double dipole reached in (π^+, π^-) on ^{56}Fe $(T = 2)$ can have five isospin members with $0 \leq T \leq 4$ arising from coupling of $\Delta T = 2$ to the ground state. Figure 8 shows a schematic energy-level diagram of the giant dipole and double-dipole resonances observed in single and double charge exchange, respectively. The three isospin components of the charge-exchange GDR and five isospin components of the double isovector giant dipole are indicated in the figure. Simple double-isospin coupling arguments through the GDR $(T-1,\ T,\ T+1)$ (assuming all components have the same reduced matrix elements) give the following intensity ratios for the isospin multiplet:

$$\sigma(T=0) : \sigma(T=1) : \sigma(T=2) : \sigma(T=3) : \sigma(T=4)$$

$$= 0.20 : 0.75 : 0.74 : 0.19 : 0.014.$$

These values are indicated as $(\sum C_1\, C_2)^2$ in the figure. Therefore about 90% of the total strength concentrates in the $T = 0$, 1, and 2 components. The reduced matrix elements will further suppress the upper isospin members due to Pauli blocking. Thus, most of the double dipole strength concentrates in the lowest three members. In the ^{56}Fe$(\pi^-, \pi^+)^{56}$Cr reaction a double-dipole state will have only one isospin component with the highest value $(T = 4)$. The difference between the centroid energies of the double-dipole resonance in the two reactions can be written as

$$Q(\pi^-, \pi^+) - Q(\pi^+, \pi^-) = 4(\Delta E_C - \Delta m_{np}) - \Delta E_S\ ,$$

where ΔE_C is the Coulomb displacement energy, $\Delta m_{np} = 1.29$ MeV is the neutron–proton mass difference and ΔE_S is a symmetry energy. Substituting[17] $\Delta E_C = 8.937$ MeV we obtain $\Delta E_S = 10.0 \pm 1.4$ MeV. This symmetry energy seems reasonable. It exceeds the isospin splitting $\Delta E(T+1, T-1) = 5.1 \pm 3.1$ MeV derived by comparing (π^+, π^0) and (π^-, π^0) data on ^{60}Ni (Ref. 15). It should be emphasized, however, that in the SCX case, ΔE is the energy splitting between $T = 3$ and predominantly

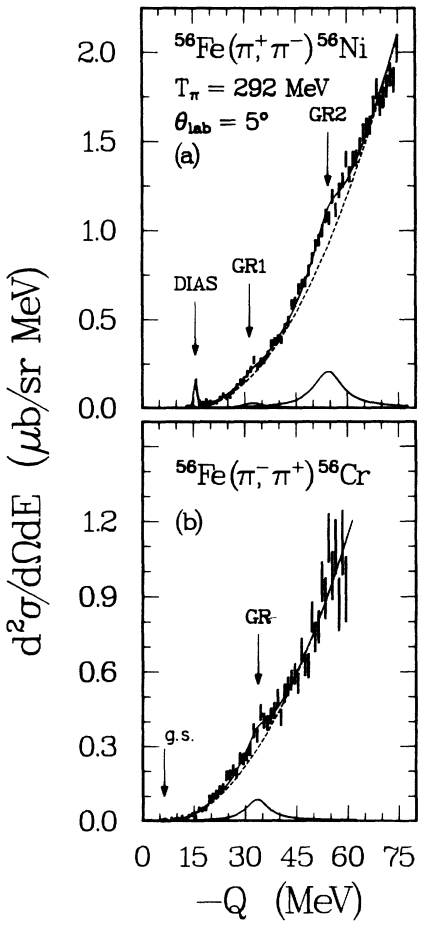

FIG. 7. (a) Same as Fig. 3 except for $\theta_{lab} = 5°$. (b) Same as above except for the inverse reaction ^{56}Fe(π^-, π^+). The arrows indicate the fitted location of the ground state (g.s.) and the giant resonance (GR).

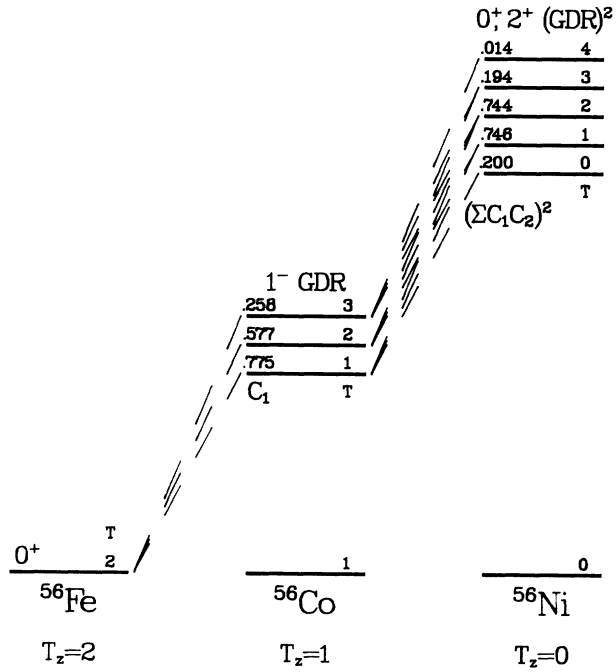

FIG. 8. Schematic energy-level diagram and isospin splitting of the single dipole (GDR) and the double-dipole (GDR^2) states anticipated in single- and double-charge exchange reactions.

$T=1$ members of the GDR, while in DCX the energy splitting is between the $T=4$ member and the energy centroid of the double-dipole quintet (which is expected to be somewhere between the $T=1$ and $T=2$ members).

The cross-section ratio $\sigma(\pi^+, \pi^-)/\sigma(\pi^-, \pi^+) \approx 3.0$ for the double dipole on ^{56}Fe arises from Pauli blocking in changing two protons into two neutrons. SCX data[15] to the GDR on ^{60}Ni (same isospin as for ^{56}Fe) give a ratio of $\sigma(\pi^+, \pi^0)/\sigma(\pi^-, \pi^0) = 2.2$. Thus, our cross-section ratio is about 40% larger than in SCX, indicating that the overall blocking effect in the (π^-, π^+) reaction on ^{56}Fe is larger than in SCX but less than the square of the SCX ratio. The Q-value effect between the two DCX modes is found to be only about 5% at 292 MeV. Taking into account the Q-value effect will increase the above ratio to 45%. Table III also shows that the width of the double-dipole states is larger than those observed for the GDR in SCX by a factor of about 1.5 → 2.0. This is in good agreement with theoretical estimates for the widths of the double-dipole resonances in terms of two phonon states, as discussed in Sec. III E.

E. Widths of double-dipole resonances

More than 15 years ago an expression for the width of the first known double giant resonance, the DIAS, was derived.[18] The result was that for nuclei with a large neutron excess ($N - Z >> 1$) the width of the DIAS is twice the width of the "single" isobaric analog state (IAS):

$$\Gamma_{\mathrm{DIAS}} \approx 2\Gamma_{\mathrm{IAS}} \ . \tag{7}$$

The derivation of this relation is based on the following considerations. The width of the IAS is mainly due to its coupling to the $T-1$ component of the isovector monopole resonance,[18,19] $|M\rangle$ in the $\Delta T_z = -1$ nucleus. This coupling gives rise to its width. Analogously, the DIAS width results from its coupling to the $T-1$ component (i.e., $T_-|M\rangle$) of the isovector monopole in the $\Delta T_z = -2$ nucleus member of the isobaric multiplet. Assuming that the analog nucleus has the same density of $T-1$ states and that the energy difference between the IAS and $|M\rangle$ is the same as the DIAS and $T_-|M\rangle$, (both quite reasonable assumptions) it was possible to express the ratio of the widths of the DIAS and IAS as

$$\frac{\Gamma_{\mathrm{DIAS}}}{\Gamma_{\mathrm{IAS}}} \approx \frac{2(2T-1)}{2T-2} \ . \tag{8}$$

In the limit of large T (i.e., $N - Z$) one obtains the relation in Eq. (7). Taking this limit means of course that the IAS and DIAS can be viewed as collective one- and two-phonons correspondingly of isospin vibrational motion. This idea was generalized recently[20] to any two (or many) independent phonon states (see also Ref. 21).

The width of a collective one-phonon state, $|1;\lambda\rangle$ (but also of any other state) is obtained by coupling it to all other states and writing

$$\Gamma_{1;\lambda} = 2\pi\rho \sum_{\alpha} |\langle 1;\lambda|V|\alpha\rangle|^2 \ , \tag{9}$$

where the sum runs, in principle, over all states $|\alpha\rangle$ different from $|1;\lambda\rangle$, and ρ is the density of states α in the vicinity of the phonon state.

In Ref. 20 this expression is treated in the "doorway" state approximation. The sum in Eq. (9) is replaced by a single "doorway," which by itself carries a width, i.e.,

$$\Gamma_{1;\lambda} = \frac{|\langle d|V_{d,\lambda}|1;\lambda\rangle|^2}{(\hbar\omega_\lambda - E_d)^2 + \Gamma_d^2/4}\Gamma_d \ , \tag{10}$$

where $\hbar\omega_\lambda$ is the energy of the phonon state of type λ, and E_d and Γ_d are the energy and width of the doorway. Going over to a state of n independent phonons of type λ, i.e., $|n;\lambda\rangle$, one can now ascribe the width to the coupling of this n-phonon state to a state of $(n-1)$ phonons and the state $|d\rangle$. The width of the n-phonon state is now given by[20]

$$\Gamma_{n;\lambda} = \frac{|\langle n-1;\lambda, d|V_{d\lambda}|n;\lambda\rangle|^2}{[n\hbar\omega_\lambda - (n-1)\hbar\omega_\lambda - E_d]^2 + \Gamma_d^2/4}\Gamma_d \ . \tag{11}$$

It is easy to see[20-22] that the matrix element in the numerator can be written as

$$\langle n-1;\lambda, d|V_{d\lambda}|n;\lambda\rangle = \sqrt{n}\langle d|V|1;\lambda\rangle \ . \tag{12}$$

Thus

$$\Gamma_{n;\lambda} = \frac{n|\langle d|V|1;\lambda\rangle|^2}{(\hbar\omega_\lambda - E_d)^2 + \Gamma_d^2/4}\Gamma_d \ . \tag{13}$$

Comparing Eq. (10) and Eq. (13) we find

$$\Gamma_{n;\lambda} = n\Gamma_{1;\lambda} \ . \tag{14}$$

The physical meaning of this result is very simple. Each of the n identical phonons can decay independently into the "doorway" state $|d\rangle$ giving rise to a width which is n times the width of a single-phonon state.

For $n=2$ we have

$$\Gamma_{2;\lambda} = 2\Gamma_{1;\lambda} \ . \tag{15}$$

On this basis we should expect the double-dipole states to be twice as wide as the single-dipole state. Indeed, in Table III, the widths observed in our DCX experiments are about a factor of 1.5–2.0 larger than the widths observed in pion SCX reactions.

Expression (15) is of course an approximation. The assumption that the double resonances represent fully independent phonons is of course violated to a certain degree. Anharmonicity effects leading to all kinds of splittings (because of isospin, deformation, etc.) are well known to alter the simple phonon picture. Also, penetrability effects and in particular single-particle fragmentation due to loss of collectivity (the so-called Landau damping) will all affect the expression in Eq. (14). Still, this relation should provide a guideline when one tries to estimate widths of two- (or multi-) phonon states and assessing the possibilities of observing such states.

F. Mass dependence of the double giant dipole resonance

An interesting question is how the cross section of the double-dipole state varies as a function of N, Z, and A. The results from pion SCX data to the single dipole provide a guide when trying to estimate the strength at which the double dipole is expected to appear. The non-spin t_{-1} (t_{+1}) mode of the GDR has been observed to be strongly populated in the (π^+, π^0) [(π^-, π^0)], charge exchange reaction.[5,15,16] Table III shows some of the existing ($\pi^{\pm}$, π^0) SCX data at 165 MeV from Ref. 15. We note that except for the GDR on ^{40}Ca, which has only one ($T=1$) isospin member, the GDR cross sections on the heavier targets reported in Ref. 15 include all three isospin members ($T-1$, T, and $T+1$) which are not resolved with the π^0 spectrometer. Our best fit to the summed GDR cross sections gives[11]

$$d\sigma/d\Omega_{\rm GDR}(\text{peak}) = (1606 \pm 27)\frac{NZ}{A^{1.84}}\ \mu\text{b/sr}\ , \qquad (16)$$

where we have included the expected NZ factor. The fit to the data using Eq. (16) is shown in Fig. 8 of Ref. 11. The predicted cross section for the GDR at 292 MeV based on the data at 165 MeV gives virtually the same N, Z, and A dependence,[11] except for a scaling factor of about 2.8, which is due to a k^2 factor.[16] Equation (16) implies a very weak A dependence of the maximum GDR cross section since $NZ \approx A^2$. In contrast to the almost constant cross section for the GDR (0.7 → 0.9 mb/sr), the cross sections for the double dipole (which are 2–3 orders of magnitude weaker than the "single" GDR) increase steadily with A by about a factor of 2 from ^{40}Ca to ^{197}Au. A qualitative argument to understand this feature can be given by breaking the cross section for the GDR^2 as a product of strength times an attenuation factor due to the distortion of the pion waves inside the nuclear medium. If we use the $E1$ classical sum rule for the dipole,[22]

$$S(E1) = 14.8\frac{NZ}{A} = |M(E1)|^2\, E\, e^2\,\text{fm}^2\text{MeV}\ , \qquad (17)$$

where $|M(E1)|^2$ is the dipole transition strength, which for $E \simeq A^{-1/3}$ gives

$$|M(E1)|^2 \simeq \frac{NZ}{A^{2/3}}\ . \qquad (18)$$

One can factor the GDR cross section as

$$d\sigma/d\Omega_{\rm GDR} \approx |M(E1)|^2 \times A^{-\alpha}\ . \qquad (19)$$

Results of Eq. (16) together with Eq. (19) give $\alpha = 1.17$.

Including the previous data on ^{32}S, the existing data on the GDR^2 consists of the nine (π^+, π^-) data points listed in Table III. The 5° cross sections listed in the table are for fitting the resonance as a whole with a single peak with the listed width. We note that in the deformed nuclei ^{12}C, ^{13}C, and ^{32}S, studied in the present and previous work[1], the double dipole splits due to deformation corresponding to vibrations along the major and minor axes. In ^{13}C the GDR^2 is expected to have additional splitting due to isospin. In the preceding nuclei the double dipole was also fit with a single peak in order to study the global features of the resonance. The 5° cross sections for the double-dipole resonance are well represented (Fig. 9) by the function

$$d\sigma/d\Omega_{\rm GDR^2}(5°) = 10\,150\frac{(NZ)^2}{A^{3.61}}\ \mu\text{b/sr}\ . \qquad (20)$$

The fit in Fig. 9 does not include the ^{12}C and and ^{32}S deformed nuclei. The result of Eq. (20) is interesting in view of the regularities for the GDR pointed out earlier. It is likely that the $(NZ)^2$ factor arises from the two-step GDR form factor. One can similarly break the cross section for the GDR^2 as the product of the strength of the first and second step times an overall attenuation factor for DCX

$$d\sigma/d\Omega_{\rm GDR^2} \approx \left(\frac{NZ}{A^{2/3}}\right)^2 A^{-\alpha'}\ . \qquad (21)$$

A comparison of Eqs. (20) and (21) yields $\alpha' = 2.28$. This attenuation factor is slightly larger than $\alpha' = 1.67$, deduced from the systematics of the GDR built on the IAS.[11] Therefore the average pion attenuation in DCX from the two types of double resonances ($\overline{\alpha'} = 1.97$) is about 73% larger than the average attenuation factor for SCX ($\overline{\alpha} = 1.14$) leading to the GDR or to the IAS. This is quite interesting and may be attributed to the fact that pion DCX involves three-pion propagations whereas only two-pion propagations are involved in the SCX reaction. A more theoretical approach for double-giant resonances in nuclei is highly desirable in order to understand these phenomena.

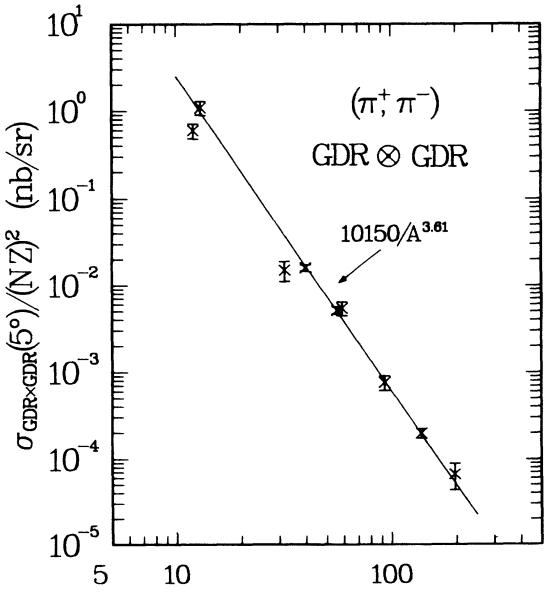

FIG. 9. Plot of normalized cross section vs A for the double-isovector giant dipole state measured in the present and previous DCX reactions at 292 MeV. The line is a power-law fit to the data of Eq. (20) (see the text).

IV. SUMMARY

We have reported the observation of double-isovector giant dipole resonances in both (π^+, π^-) and (π^-, π^+) reactions. The double dipole appears at about twice the energy of the one-step GDR observed in pion SCX and its width is about twice the width of the "single" dipole. Angular distributions were measured for the double dipole on ^{40}Ca, ^{56}Fe, and ^{93}Nb and found to have a quadrupole shape; however, the data may indicate that we actually observe both the 0^+ and 2^+ members of the double dipole. In (π^-, π^+) the double dipole appears at about four Coulomb energies lower than in the (π^+, π^-) reaction (after correcting for the symmetry energy), and is suppressed by the Pauli-blocking effect. The data from the present and recent studies indicate that the double giant dipole resonance is a general collective feature of nuclei and has a simple mass dependence. This work indicates that pion DCX is a unique reaction to identify the double-isovector giant resonances in nuclei.

ACKNOWLEDGMENTS

We thank M. Johnson, M. Singham, H. Baer, and D. Bowman for stimulating discussions. This work is supported by the U.S.–Israel Binational Science Foundation, the Robert A. Welch Foundation, the National Science Foundation, and the U.S. Department of Energy.

[1] S. Mordechai *et al.*, Phys. Rev. Lett. **61**, 531 (1988).
[2] N. Auerbach, Proceedings of the LAMPF Workshop on Photon and Neutral Meson Physics at Intermediate Energies, Los Alamos, 1983 (unpublished); Proceedings of the Workshop on Pion-Nucleus Physics: Future Direction and New Facilities at LAMPF, Los Alamos, 1987 (unpublished).
[3] S. Mordechai *et al.*, Phys. Rev. Lett. **60**, 408 (1988).
[4] S. Mordechai *et al.*, Phys. Rev. C **38**, 2709 (1988).
[5] H. W. Baer *et al.*, Phys. Rev. Lett. **49**, 1376 (1982).
[6] U. Sennhauser *et al.*, Phys. Rev. Lett. **51**, 1324 (1983).
[7] H. W. Baer *et al.*, Phys. Rev. Lett. **45**, 982 (1980).
[8] H. A. Thiessen *et al.*, Los Alamos Scientific Laboratory Report No. LA-6663-MS, 1977 (unpublished); S. J. Greene *et al.*, Phys. Lett. **88B**, 62 (1979).
[9] C. L. Morris *et al.*, Nucl. Instrum. Methods A **238**, 94 (1985).
[10] G. Rowe, M. Salomon, and R. H. Landau, Phys. Rev. C **18**, 584 (1978).
[11] S. Mordechai *et al.*, Phys. Rev. C **40**, 850 (1989).
[12] S. A. Wood, Los Alamos National Laboratory Report No. LA-9932-T, 1984 (unpublished).
[13] J. L. Matthews, Proceedings of the LAMPF Workshop on Pion Double Charge Exchange [Los Alamos National Laboratory Report No. LA-10550-C, 1985 (unpublished)].
[14] E. Rost, computer code CHOPIN (unpublished). The code has been modified by one of us (C.L.M) to calculate pion charge exchange reactions and renamed NEWCHOP.
[15] A. Erell *et al.*, Phys. Rev. C **34**, 1822 (1986).
[16] F. Irom *et al.*, Phys. Rev. C **34**, 2231 (1986).
[17] M. S. Antony, J. Britz, and A. Pape, At. Data Nucl. Data Tables **40**, 9 (1988).
[18] N. Auerbach, Phys. Lett. **41B**, 403 (1972).
[19] N. Auerbach, Phys. Rep. **98**, 273 (1983).
[20] N. Auerbach (unpublished).
[21] G. Baur and C. A. Bertulani, *The Response of Nuclei Under Extreme Conditions*, edited by R. A. Broglia and G. F. Bertsch (Plenum, New York, 1988).
[22] A. Bohr and B. R. Mottleson, *Nuclear Structure* (Benjamin, New York, 1975), Vol. 2.